AIAA JOURNAL
Vol. 31, No. 3, March 1993

Fundamental Turbulence Measurements by Relief Flow Tagging

Richard B. Miles,* Deyu Zhou,† Boying Zhang,† and Walter R. Lempert‡
Princeton University, Princeton, New Jersey 08544
and
Zhen-Su She§
University of Arizona, Tucson, Arizona 85721

The observation of small-scale velocity structures in high Reynolds number turbulent flowfields is important for the understanding of energy scaling and dissipation phenomena. The Raman excitation plus laser-induced electronic fluorescence (RELIEF) technique is shown to be a promising tool to observe these scales. Lines on the order of 100 μ thick and 1 cm long are written into a contained turbulent jet and observed with a resolution on the order of tens of microns. The images that are recorded give instantaneous velocity profiles if very short time delays between tagging and interrogation are used. This time-of-flight approach is a direct measure of velocity, so approximations such as constant density, constant temperature, or the Taylor hypothesis are not required. The velocity data are analyzed to yield the velocity profile, the turbulence intensity, the lateral correlation function, and the lateral second-order structure function. At 35 jet exit diameters downstream, a slope of 0.669 is measured through the inertial subrange portion of the ℓn-ℓn plot of the second-order structure function.

I. Introduction

IN discussions with Frisch and others, it has been pointed out that the Raman excitation plus laser-induced electronic fluorescence (RELIEF) technique is a particularly powerful tool for studying turbulent structures in air flows. By writing a line across a flow one can measure spatial information about the turbulent flow structure at a single point in time. This complements the data provided by a hot-wire probe that generates time-varying information at a single point in space. For measurement of turbulent flow parameters, the hot-wire probe has several limitations:

1) To convert the time-varying signal to a spatially varying velocity, the Taylor hypothesis must be invoked. It has been shown that this hypothesis overestimates the spatial variation in high-intensity turbulence.[1]

2) The finite size of the hot-wire probe (on the order of 0.5 mm) makes it impossible to measure fluctuations down to the Kolmogoroff scale, which is on the order of 10 μ to 100 μ in most flowfields.

3) The hot-wire probe does not directly measure the velocity, so temperature and density effects must be eliminated by measurements at different overheat ratios or by approximation.

Other nonintrusive approaches for measuring turbulent flow parameters usually rely on particle seeding. Because of the inability of particles to follow high-frequency fluctuations, these approaches are not satisfactory for looking at small-scale phenomena. Furthermore, the noncontinuous nature of the measurement makes spatial and temporal correlations difficult to achieve. Laser-induced fluorescence can be used to observe turbulence phenomena, but it requires that flowfields be seeded and that the seed concentration be uniform.[2]

Presented as Paper 92-0007 at the AIAA 30th Aerospace Sciences Meeting, Reno, NV, Jan. 6-9, 1992; received March 3, 1992; revision received Aug. 24, 1992; accepted for publication Sept. 3, 1992.

*Professor, Mechanical and Aerospace Engineering. Senior Member AIAA.
†Graduate Student, Mechanical and Aerospace Engineering.
‡Research Scientist, Mechanical and Aerospace Engineering. Member AIAA.
§Associate Professor, Department of Mathematics.

Although the RELIEF technique is applied here in a relatively small-scale facility, it may also be extended to larger scales. The tagging process does not significantly deplete the pump laser beams, so lines can be written into full-scale facilities. The interrogation process involves photons that are only absorbed by vibrationally excited oxygen molecules, so the interrogation laser beam is not significantly attenuated unless the flow is hot. The major scaling factor is the collection optics of the camera. In large-scale facilities, a large collection lens must be used so that the camera can be located out of the flowfield. As long as optical access is available, the RELIEF technique can be applied to air flows of arbitrary complexity.

II. Relief Method

To examine the application of the RELIEF flow tagging technique to the study of turbulence, we have made measurements in a contained small-scale turbulent jet.[3] The apparatus that is used is shown in Fig. 1. It includes a frequency-doubled, high-power (300 mJ/pulse) Nd:YAG laser plus a Raman shifter that generate the 532-nm (green) and 581-nm (orange) tagging beams.[4] Tagging takes approximately 10 ns and is accomplished by driving the oxygen molecules into their first vibrationally excited state using stimulated Raman scattering.

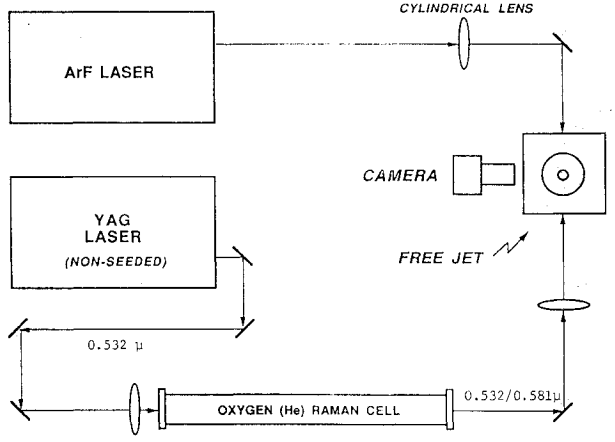

Fig. 1 Instrumental schematic for RELIEF flow tagging studies of freejet turbulence.

The tagged line is on the order of 100 μ wide (full width at half-maximum) and a few centimeters long. This line then moves downstream for a short time interval, whereupon it is interrogated by a 50-mJ/pulse, 193-nm ArF laser which illuminates the volume surrounding the line. This ultraviolet light further excites the tagged oxygen molecules to the Schumann-Runge band from which they fluoresce, emitting near ultraviolet (200–400 nm) light. The laser-induced electronic fluorescence is then imaged on a high-sensitivity uv camera. As a result of rapid predissociation, fluorescence occurs immediately, so the interrogation time is just the pulse duration of the argon-fluoride laser, approximately 10 ns.

A molecular time-of-flight measurement of velocity such as this is a primary standard approach since it directly measures the velocity and is not affected by other flow parameters such as temperature and density. Indirect measurements of velocity such as those based on particles (laser Doppler velocimetry, particle imaging velocimetry, etc.), and those based on cooling rates (hot wire, thin film, etc.) are secondary standard approaches since they do not actually observe the motion of the air itself. Spectroscopically based molecular velocimetry measurements rely on the Doppler shift and are subject to errors arising from pressure induced frequency shifts and temperature fluctuations.

In the RELIEF measurements, the time interval between tagging and interrogation can be varied depending on the requirements of the experiment. When a turbulent flowfield is being observed, the time must be short compared to the characteristic time of the highest frequency eddies to avoid inaccuracies due to line stretching or roll-up. Longer time intervals may be used to visualize the velocity profile or turbulent structure, and may be appropriate for wavelet analysis or other types of direct measurements of flow structure. With the current laser system, the line can only be interrogated a single time. With future lasers, it may be possible to interrogate one line at multiple time intervals, or to write sequential lines to observe the time-evolving character of the flow. In the current experiments, however, each tagging-interrogation sequence is separately recorded and statistics are built up by repeating the sequence at the laser pulse repetition rate of approximately 10 Hz.

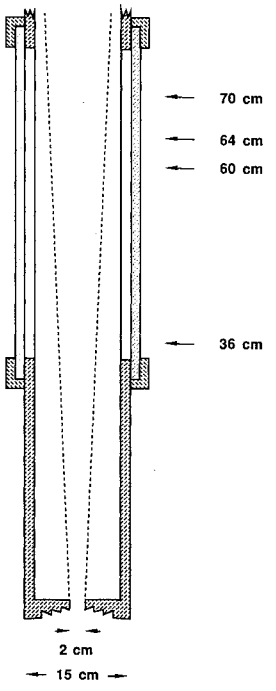

Fig. 2 Schematic diagram of freejet test chamber.

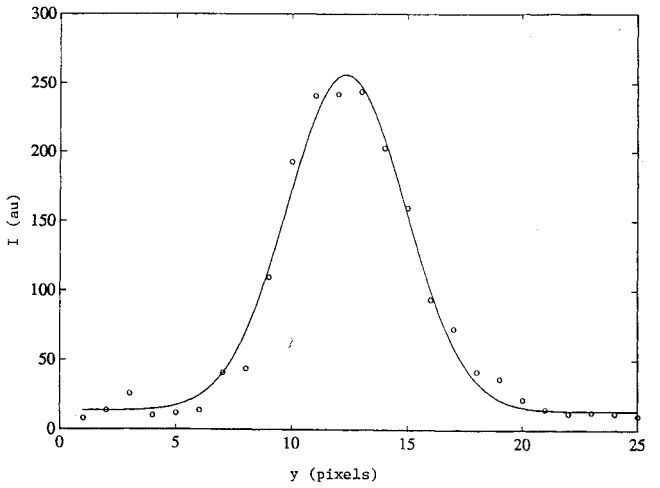

Fig. 3 Experimental data (points) and Gaussian fit (solid curve) at one location across the displaced line segment for the flow marked at the 60 cm location; time delay is 5 μs, the full width at half-maximum is 6.0 pixels, corresponding to 97 μ.

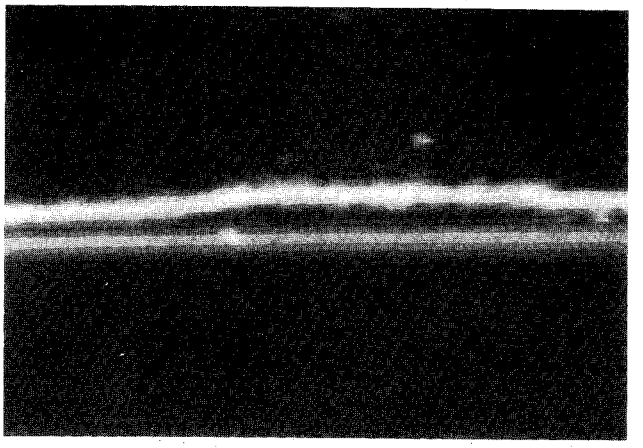

Fig. 4 Example of the original tagged lines (lower) and line displaced after 5 μs (upper) at the location 60 cm downstream of the jet exit.

III. Experimental Setup

The flow facility consisted of a 2-cm-diam circular jet exiting into a square cross section (15 × 15 cm) open-ended channel. Experiments were conducted at locations 36 cm (18 diameters), 60 cm (30 diameters), 64 cm (32 diameters), and 70 cm (35 diameters) downstream of the nozzle, with the largest data set (4774 frames) taken at the 60-cm location. A sketch of the test chamber apparatus is shown in Fig. 2. The stagnation chamber was operated at 10 psi higher than atmospheric pressure, leading to a pressure ratio of 1.7 between the plenum and the channel exit. The air temperature in the plenum was approximately 270 K, somewhat lower than room temperature due to expansion cooling. The jet exit velocity into the test chamber was computed to be approximately 275 m/s, leading to an exit Reynolds number of 5.5×10^5 based on the jet diameter. Using the relationship given by Antonia et al.[5]

$$R_\lambda \cong 1.74\, R_{\text{exit}}^{1/2} \tag{1}$$

we expect that R_λ (the Reynolds number based on the Taylor microscale) will be 1.3×10^3, assuming our jet has characteristics similar to those of a free jet. This may not be a good assumption since the exit velocity is high (~ Mach 0.8), so compressibility effects occur. Our jet is also enclosed in a channel, leading to a streamwise adverse pressure drop that causes recirculation along the walls and reduces the average jet velocity in the far field.

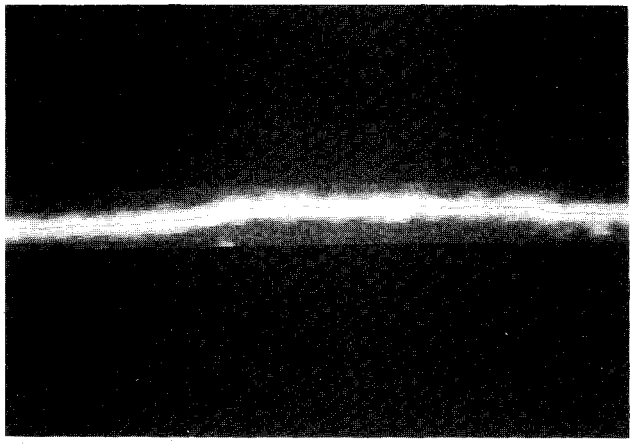

Fig. 5 Displaced line with the computer-identified line center highlighted.

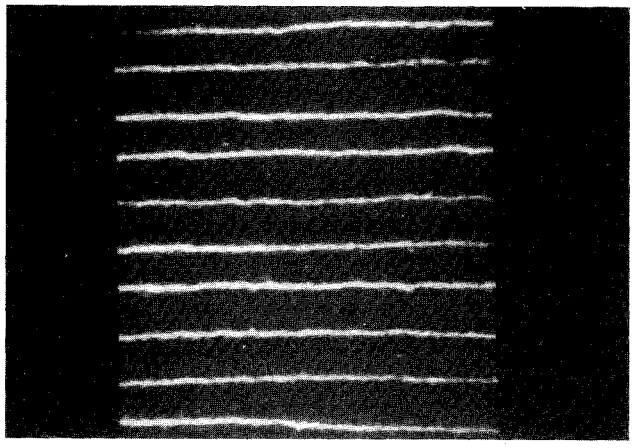

Fig. 6 Collage of 10 displaced lines all taken with a 5-μs delay at the 60-cm downstream location.

The camera system was set up so that the line image was somewhat magnified to enable us to resolve down to approximately the Kolmogoroff scale. Because of the finite number of pixels across the image plane, the magnification determines the range of scales observed. For example, typical line segments analyzed at the 60-cm location were 0.6 cm long and had a full width at half-maximum of 97 μ. This corresponded to 310 pixels along the line (49.2 pixels/mm horizontal) and 6.0 pixels across the line (61.8 pixels/mm vertical). Longer line segments could be measured, but, due to the finite resolution of the camera, this would lead to less accurate measurement of small-scale structures.

The line profile is Gaussian due to the Gaussian profile of the tagging lasers. Thermal diffusion preserves the Gaussian profile and accounts for a broadening of approximately 5% in 5 μs. If the line is thin compared to the turbulence scale, and the time interval is short, the line profile can be assumed to be Gaussian at the time of interrogation. Thus, we use a Gaussian fitting program to locate the line center at each point along the line. An example of that Gaussian fit is shown in Fig. 3. The dots represent experimental points and the line shows the Gaussian-fitted profile. The center of the Gaussian fit corresponds to the center of the line. With this approach, the center of the line can be found to better than 0.2 pixels (3 μm). Figure 4 shows an example of a displaced line segment taken at the 60 cm downstream location using a 5-μs delay between tagging and interrogation. The original tagged line is also shown on the plate to give an indication of the displacement between tagging and interrogation. Figure 5 shows the same line segment with the computer-identified line center highlighted. Figure 6 is a collage of many similar lines. Several thousand lines were analyzed at each measurement location to generate the turbulence data presented here.

IV. Experimental Results

Figures 7a, 7b, 8a, 8b, and 9a, 9b show the velocity profiles and turbulence intensity profiles at 36, 60, and 70 cm downstream, respectively. The asymmetry in these profiles arises because the sample line was not always located in the exact center of the jet. At 36 cm downstream, the average centerline velocity was 112.8 m/s. By 60 cm downstream, that had slowed to 23 m/s, and at 70 cm was only 3.8 m/s, as indicated in the figures. This rapid decrease in average velocity occurs due to the adverse pressure gradient in the enclosed channel. Whereas some variation in the velocity across the jet was seen at each of these locations, the turbulence intensity u' was constant across the jet at all stations as shown in the figures. The averaged values for u' were 34.0 m/s at 36 cm, 17.2 m/s at 60 cm, 13.1 m/s at 64 cm, and 10.0 m/s at 70 cm. Note that the flow was reversed a significant fraction of the time at the 70-cm location. In contrast to some other velocity measurement techniques, flow reversal has no effect on the RELIEF data analysis. These values of u' and an R_λ of 1.3×10^3 give expected Taylor microscales of 430 μ at 36 cm, 850 μ at 60 cm, 1.10 mm at 64 cm, and 1.50 mm at 70 cm, assuming a freejet expansion.

Figures 7c, 8c, and 9c show the lateral correlation functions $g(x, \Delta x)$ with x chosen at the midpoint of the line. The lateral correlation function is given by the expression

$$g(x, \Delta x) = \frac{\frac{1}{m}\sum_{i=1}^{m}[u_i(x) - \overline{u(x)}][u_i(x + \Delta x) - \overline{u(x + \Delta x)}]}{u'(x)u'(x + \Delta x)} \quad (2)$$

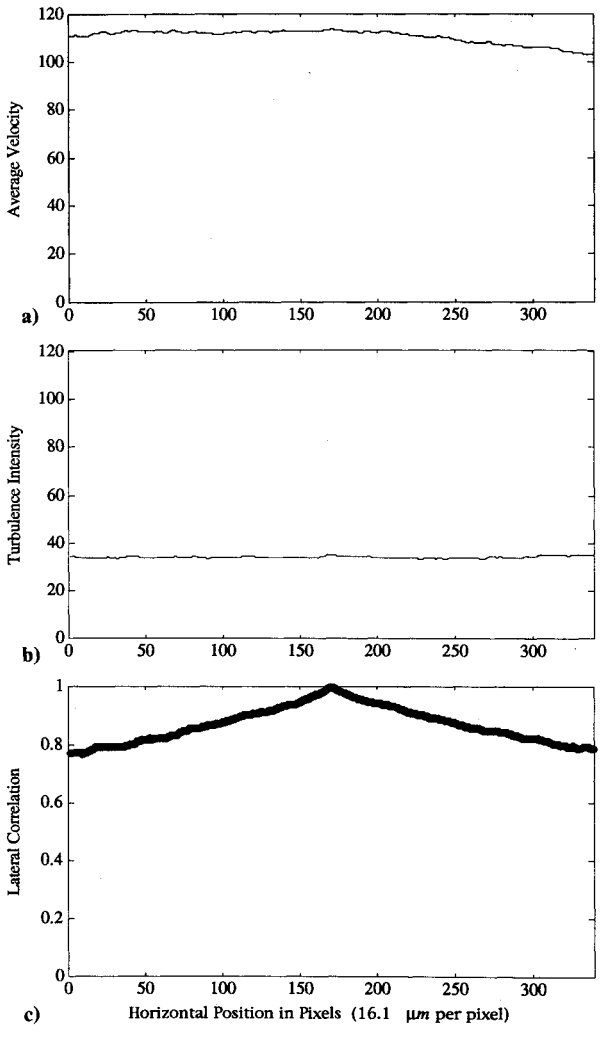

Fig. 7 Contained freejet at 36 cm downstream of the jet exit (3-μs delay between tagging and interrogation): a) mean velocity (m/s), b) turbulence intensity (m/s), and c) lateral correlation function.

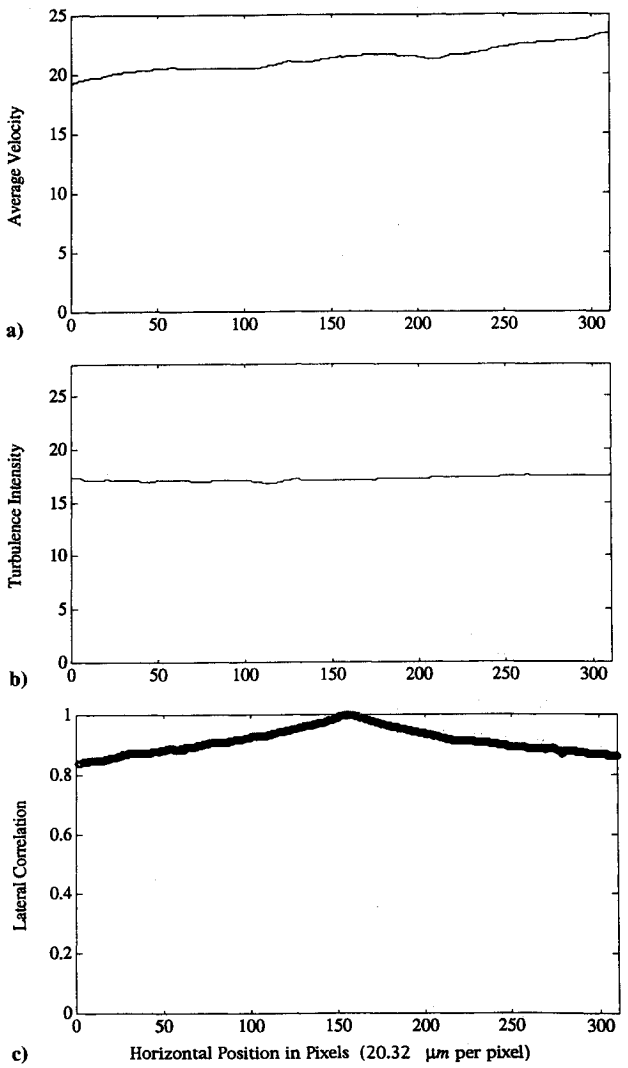

Fig. 8 Contained freejet at 60 cm downstream of the jet exit (5-μs delay between tagging and interrogation): a) mean velocity (m/s), b) turbulence intensity (m/s), and c) correlation function.

where the sum is over m images (1216 at 36 cm, 4774 at 60 cm, 1510 at 64 cm, and 2963 at 70 cm). The measured axial velocity at position x, in image i, is $u_i(x)$, and the velocity at position x averaged over all images is $\overline{u(x)}$. The lateral correlation function is a statistical measure of the size of the velocity structures across the flowfield. As the lateral separation variable Δx goes to zero, the correlation function must go to 1. For a separation larger than the large structure scale, the correlation goes to zero. Note here that for the largest separations measured, the correlation is still large, indicating that the line segment observed was much smaller than the scale of the large structures in the flow.

The curvature of the correlation function around $\Delta x = 0$ gives a direct measure of the Taylor microscale λ_g.

$$\lim_{\Delta x \to 0} \{g(x, \Delta x)\} = 1 - (\Delta x^2/\lambda_g^2) \tag{3}$$

The outer curve in Fig. 10 shows a parabolic fit to the four points closest to $\Delta x = 0$ for the correlation at 60 cm. Note that the point $\Delta x = 0$ is not included in this fit since uncorrelated statistical noise will generate a small spike in the correlation function at that location. This fit gives a measured Taylor microscale at the line center of 952 μ.

Using this value of the Taylor microscale, R_λ can be found from

$$R_\lambda = \frac{u'\lambda_g}{\nu} \tag{4}$$

where ν is the kinematic viscosity. Assuming the expanded jet has cooled to 250 K, the value of R_λ is 1.44×10^3 at 60 cm. At 36 cm the Taylor microscale is 463 μ leading to an R_λ of 1.38×10^3, at 64 cm the Taylor microscale is 610 μ leading to an R_λ of 700, and at 70 cm the Taylor microscale is 607 μ leading to an R_λ of 532. This rapid drop in R_λ after 60 cm suggests that the freejet approximation is no longer valid and the flow is becoming dominated by the channel. Assuming constant density, the average channel flow velocity is expected to be approximately 4 m/s. The Kolmogoroff scale can be found from the expression[6]

$$\eta = \frac{\nu}{u'} \frac{R_\lambda^{1/2}}{15^{1/4}} \tag{5}$$

This gives 6.5 μ at 36 cm, 13.3 μ at 60 cm, 12.1 μ at 64 cm, and 14.1 μ at 70 cm.

We have also used the velocity data to calculate the second-order structure function

$$f^{(2)}(\Delta x) = \langle [u(x) - u(x + \Delta x)]^2 \rangle \tag{6}$$

where $\langle\ \rangle$ implies averaging over all values of x and all images. Assuming isotropic turbulence, this structure function is directly related to the averaged lateral correlation function $\bar{g}$ by the expression

$$f^{(2)} = 2u'^2(1 - \bar{g}) \tag{7}$$

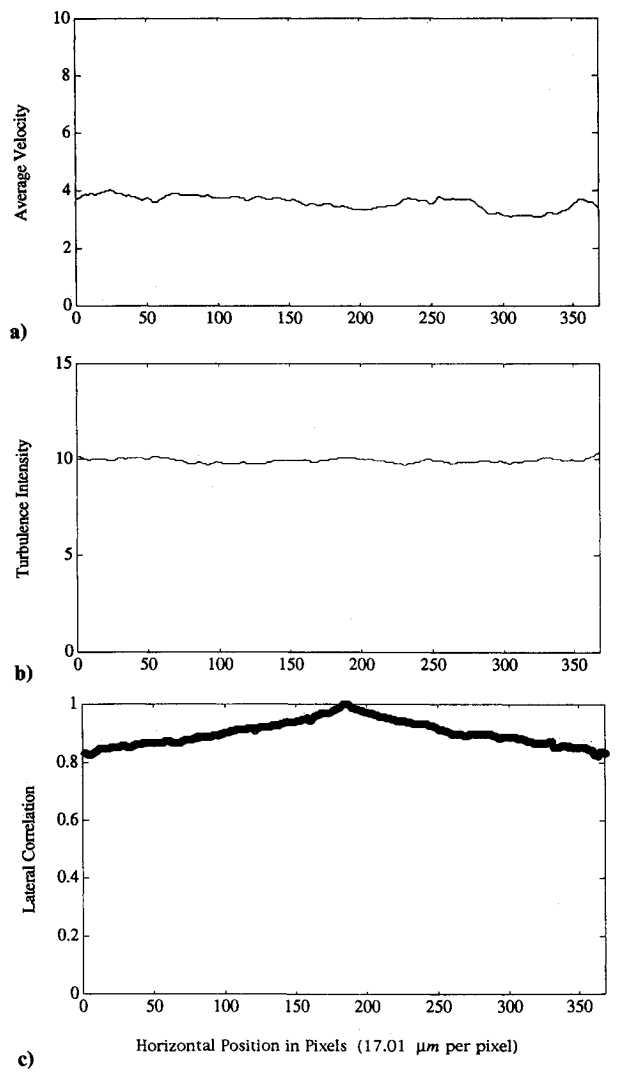

Fig. 9 Contained freejet at 70 cm downstream of the jet exit (5-μs delay between tagging and interrogation): a) mean velocity (m/s), b) turbulence intensity (m/s), and c) correlation function.

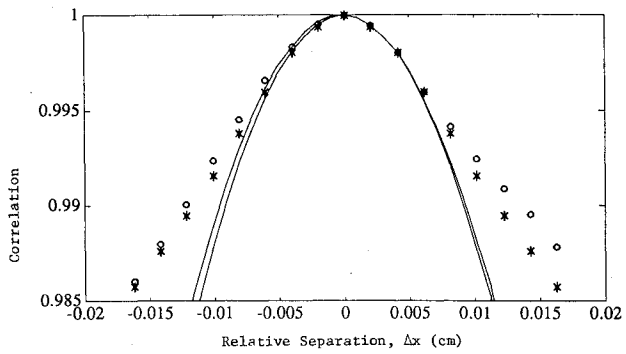

Fig. 10 Midpoint lateral correlation function near $\Delta x = 0$: o = centerline lateral correlation g, * = average correlation $\bar{g}$ calculated from the second-order structure function; curves are parabolic fits to the four data points closest to $\Delta x = 0$, excluding $\Delta x = 0$. The outer curve is the fit to g, and the inner curve is the fit to $\bar{g}$.

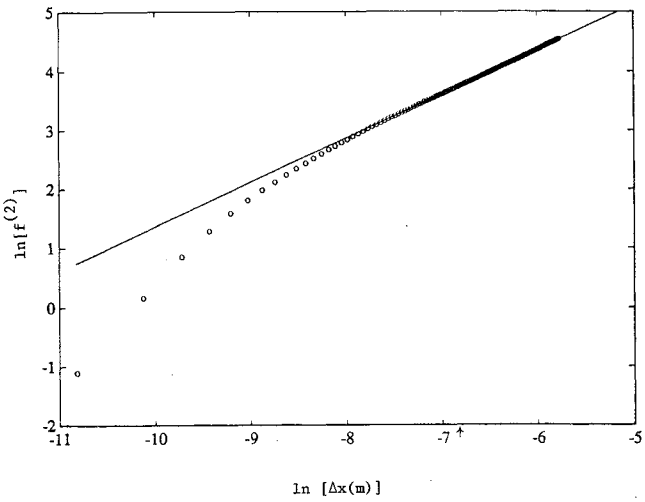

Fig. 11 Plot (ℓn-ℓn) of the second-order structure function vs Δx at 60 cm downstream of the nozzle exit. The straight line is a linear least squares fit to the linear portion of the inertial subrange and the resulting slope is 0.751. The measured value of λ_g, 952 μ, is indicated at the bottom by an arrow.

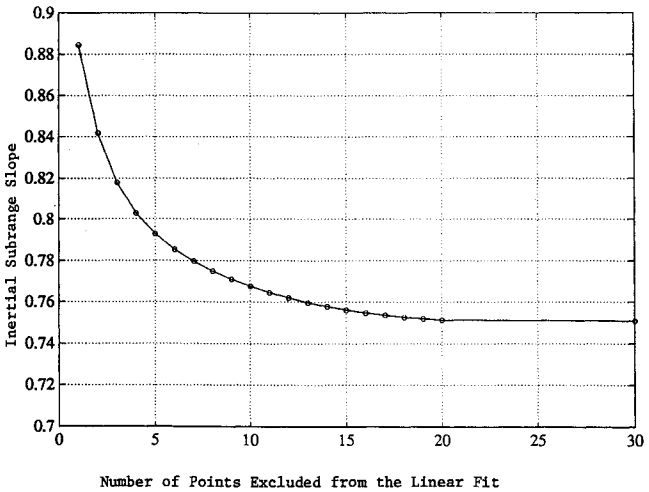

Fig. 12 Inertial subrange slope vs the number of small-scale (dissipation range) points excluded from the fit for Fig. 11: value of 0.751 is the asymptotic value and is closely approximated by excluding the first 20 points (scales smaller than 406 μ) from the fit.

By using the measured average value of u' and, again, by fitting a parabola around $\Delta x = 0$, we can find the lateral Taylor microscale averaged over the whole line. The inner curve in Fig. 10 shows this fit to the four points around $\Delta x = 0$ (not including $\Delta x = 0$) for 60 cm. From this fit we find the line averaged Taylor microscale to be 922 μ, which is somewhat smaller than the measured centerline value.

The slope of the second-order structure function is important for understanding fundamental characteristics of energy transfer in turbulence. Figure 11 shows a ℓn-ℓn plot of the second-order structure function vs Δx at the 60-cm location. The averaged Taylor microscale value is shown in the figure. The straight line portion of this plot represents the inertial subrange of energy scaling, and the point at which the deviation from the straight line occurs corresponds to the onset of viscous dissipation effects. The final slope as Δx approaches zero should approach 2 to be consistent with the symmetry requirement around the $\Delta x = 0$ point. A linear fit to the straight line section of this plot gives a slope of 0.751. This fit excludes the first 20 points of the structure function and extends to the largest scale measured, which corresponds to one-half of the sampled line length (one-half of 0.63 cm). Figure 12 shows the fitted slope as a function of the number of small-scale (dissipation range) points excluded, indicating that, by excluding the first 20 points (or 406 μ, which is 31 times the Kolmogoroff scale), the slope has converged. Figure 13 shows the convergence of the slope with the number of lines sampled. The 0.751 value of the slope is somewhat greater than the slope of 0.71 measured by Anselmet et al.[7] in both a duct and an axisymmetric freejet, however, measurements at 64 and 70 cm downstream of the nozzle yield slopes of 0.674 and 0.669, respectively. Figures 14 and 15 show convergence plots for these measurement locations. At 36 cm, the slope is

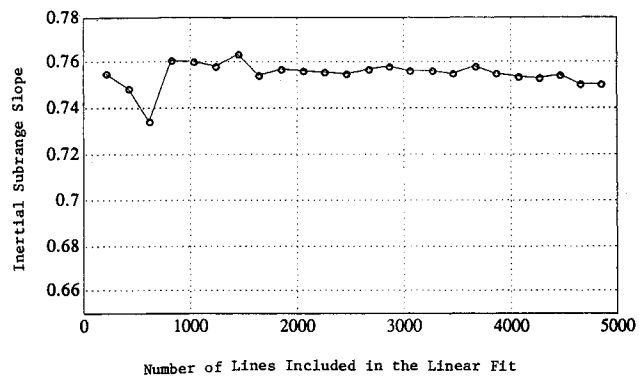

Fig. 13 Convergence of the inertial subrange slope in Fig. 11 with number of lines sampled indicating the uncertainty in the slope at 60 cm downstream of the nozzle exit is approximately 0.005.

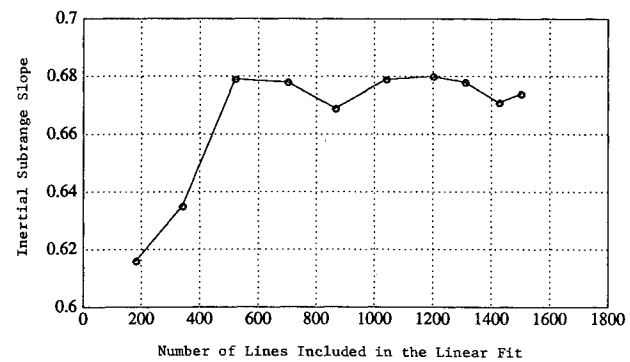

Fig. 14 Convergence of the inertial subrange slope for the point sampled at 64 cm downstream of the nozzle exit; the final value is 0.674.

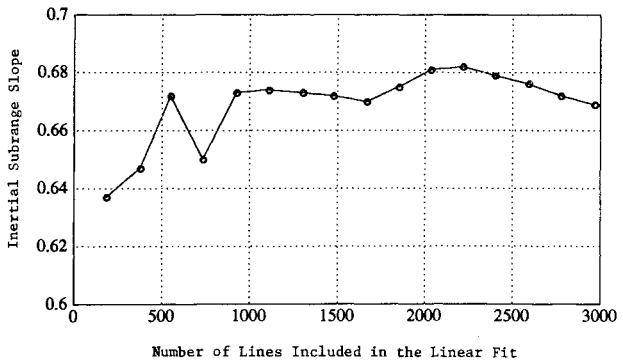

Fig. 15 Convergence of the inertial subrange slope for the point sampled at 70 cm downstream of the nozzle exit; the final value is 0.669.

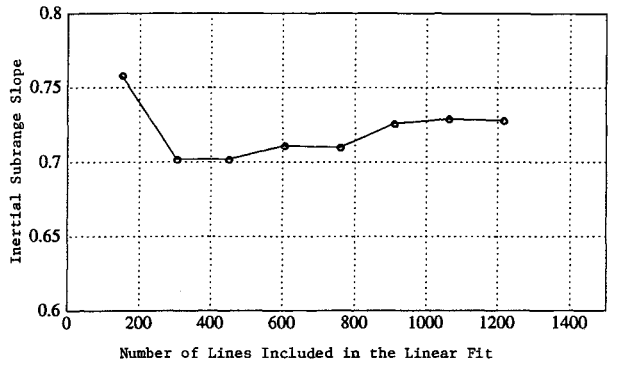

Fig. 16 Convergence of the inertial subrange slope for the point sampled at 36 cm downstream of the nozzle exit; the final value is 0.729.

0.729 as shown on the convergence plot in Fig. 16. These measurements suggest that the flow is not yet fully developed at 30 diameters, an observation consistent with that of Wyganski and Fielder[8] who performed measurements in a self-preserving freejet.

Figures 7a, 8a, and 9a show that the average velocity of the jet is not uniform across the sample line, thus the flow is not homogeneous. The second-order structure function as defined in Eq. (6) includes the contribution of a nonzero mean velocity gradient

$$f^{(2)}(\Delta x) = \langle[\bar{u}(x) - \bar{u}(x + \Delta x)]^2\rangle + \langle[U(x) - U(x + \Delta x)]^2\rangle \quad (8)$$

where $U(x)$ is the mean velocity profile and $\tilde{u}(x)$ the turbulent fluctuation. In homogeneous turbulence, the second term vanishes. In our experiment, however, the second term is nonzero. On the other hand, as seen from Figs. 7b, 8b, and 9b, the turbulence intensity is uniform, implying that the turbulent fluctuations are homogeneous. To compare our results to theories of homogeneous turbulence, we should examine the scaling exponent of the turbulent fluctuations, i.e., the first term in Eq. (8) The scaling exponents thus calculated are uniformly smaller than the values stated earlier: 0.721 at 36 cm, 0.735 at 60 cm. At 64 and 70 cm the slope remains 0.674 and 0.669, respectively, since the velocity profiles are relatively uniform and the average velocity is low compared to the turbulence intensity at these locations. We estimate that the measurement uncertainty of these slopes is ± 0.005.

V. Summary

The RELIEF flow tagging technique provides a new tool for studying fundamental turbulent phenomena in air flows. It is complementary to the hot-wire probe and yields instantaneous structural information with high resolution. By accumulating many images of displaced lines, we are able to determine the average velocity profile, the turbulence intensity, the lateral velocity correlation function, and the associated second-order structure function.

The observed decrease of the scaling exponent of the second-order structure function may reflect a progressive development of turbulent cascade: at locations farther downstream, the cascade is more maturely developed. It should be pointed out, however, that at 70 cm downstream, the jet is unlikely to be free, because of the effects of walls in the present experimental setup. A full theoretical explanation of our results remains a challenging task. It is expected that this technique will lead to new insights on the physics of energy transfer and dissipation phenomena in turbulent flows.

Acknowledgments

This work has been supported, in part, with funds contributed by Rosemount, Inc., Aerospace Division. The RELIEF diagnostic technique was developed under support from the Air Force Office of Scientific Research.

References

[1]Lumley, J. L., "Interpretation of Time Spectra Measured in High-Intensity Shear Flows," *Physics of Fluids*, Vol. 8, No. 6, 1965.

[2]Cheng, S., Zimmermann, M., and Miles, R. B., "Separation of Time-Averaged Turbulence Components by Laser-Induced Fluorescence," *Physics of Fluids*, Vol. 26, No. 4, 1983, pp. 874–877.

[3]Miles, R., Lempert, W., and Zhang, B., "Turbulent Structure Measurements by RELIEF Flow Tagging," *Fluid Dynamics Research*, Vol. 8, No. 1, 1991, pp. 9–17.

[4]Lempert, W., Zhang, B., and Miles, R. B., "Simplification of the RELIEF Flow Tagging System for Laboratory Use," AIAA Paper 91-0356, Jan. 1991.

[5]Antonia, R. A., Satyaprakash, B. R., and Hussain, A. K. M. F., "Measurements of Dissipation Rate and Some Other Characteristics of Turbulent Plane and Circular Jets," *Physics of Fluids*, Vol. 23, No. 4, 1980, pp. 695–700.

[6]Hinze, J. O., *Turbulence*, 2nd ed., McGraw-Hill Series in Mechanical Engineering, McGraw-Hill, New York, 1975, pp. 224–225.

[7]Anselmet, F., Gagne, Y., Hopfinger, E. J., and Antonia, R. A., "High Order Velocity Structure Functions in Turbulent Shear Flows," *Journal of Fluid Mechanics*, Vol. 140, March 1984, pp. 63–89.

[8]Wygnanski, J., and Fielder, H., "Some Measurements in the Self-Preserving Jet," *Journal of Fluid Mechanics*, Vol. 38, Pt. 3, March 1969, pp. 577–612.